High-efficiency solar thermophotovoltaic system using a nanostructure-based selective emitter

Rajendra Bhatt,[a] Ivan Kravchenko,[b] Mool C. Gupta[a,*]
[a]Department of Electrical & Computer Engineering, University of Virginia, Charlottesville, Virginia, 22901, USA
[b]Center for Nanophase Materials Sciences, Oak Ridge National Laboratory, Oak Ridge, Tennessee 37831, USA

Abstract. In this work, we present the design, fabrication, optimization, and experimental results of a high-efficiency planar STPV system utilizing a micro-textured absorber and a nanostructure multilayer metal-dielectric coated selective emitter fabricated on a tungsten (W) substrate. Light absorptance of more than 90% was achieved at visible and near-infrared wavelengths using the microtextured absorbing surface. The nanostructure selective emitter consists of two thin-film optical coatings of Si_3N_4 and a layer of W in between to increase the surface emissivity in spectral regimes matching the quantum efficiency of the thermophotovoltaic (TPV) cells. GaSb-based TPV cells are used in our STPV design. The experiment was conducted under solar simulation using a high-power laser diode stack. Our experimental setup measured a maximum electrical output power density of 1.71 W/cm^2 at 1676 K STPV temperature, and the overall power conversion efficiency of 8.4%, which is the highest STPV system efficiency reported so far for any experimental STPV device. The incident optical power on the absorber side was 131 W. This is equivalent to a solar concentration factor of 2060, which is within the practical limit and readily achievable with Fresnel lens setup.

Keywords: STPV, blackbody, solar cells, nanostructure, spectral control.

***Mool C. Gupta, E-mail: mgupta@virginia.edu

1 Introduction

Recently, there has been a renewed interest in the development of solar thermophotovoltaic (STPV) devices [1-4], given their potential for high-efficiency solar energy harvesting by utilizing the full solar spectrum. A single-junction solar cell is subject to the Shockley-Queisser (SQ) limit [5], which imposes a fundamental upper bound on its solar-to-electric energy conversion efficiency. According to this limit, the theoretical maximum efficiency for a single-junction cell under standard illumination (air mass of 1.5 and in the absence of concentration) is ~33% for an optimal bandgap of ~1.4 eV [6]. A major contribution to the SQ limit arises from inevitable losses (thermalization and transmission losses) caused by the spectral mismatch between solar radiation and the cell's response. STPV systems aim to achieve efficiencies higher than the SQ limit through the use of an intermediate element that absorbs the broadband sunlight and re-emits the absorbed energy as a narrow-band thermal radiation tuned to directly above the bandgap of the solar cell.

Spectrally selective absorbers and emitters can greatly enhance the STPV system efficiency by maximizing the absorption and suppressing the emission of sub-bandgap and excessive energy photons [7].

Fig. 1a shows a layout of a typical planar STPV system. Unlike conventional solar photovoltaics, STPV utilize concentrated solar radiation, which is absorbed and reemitted as thermal radiation towards a solar cell through a thermally coupled absorber and emitter pair [7]. Most of the efficiency gain of STPV arises from the spectral control in the emitter. A selective spectral filter placed in between the emitter and the solar cell reflects the sub-band-gap photons back to the emitter for recycling. An infrared (IR) reflector or heat shield can also be installed on the absorber side to minimize the thermal radiation loss from the absorbing surface [3]. Effective recycling of the unused thermal radiation greatly enhances the system efficiency. Another key aspect of designing a STPV system is choosing the bandgap of the PV cells. An optimal bandgap is determined by the thermal emission spectrum, which in turn is controlled by the emitter temperature and the spectral characteristics of the emitter surface [8]. Low bandgap cells (<1eV) are preferred because they require lower operating temperatures (<1800 K) for the emitter. Ge, GaSb, and InGaAsSb cells are of considerable interest for STPV applications. Figure 1b illustrates the impact of the STPV temperature on the conversion efficiency of GaSb PV cells. The blackbody power density at temperatures 1100K, 1400K, and 1700K are shown along with the bandgap wavelength (λ_{BG}) of GaSb. With increasing temperature, the overall radiated power per unit area increases and the peak of the blackbody curve shifts towards shorter wavelengths. Because only photons having wavelengths less than λ_{BG} can be converted to electric energy, the maximum thermal-to-electrical conversion efficiency is limited by the fraction of the total radiated power that is below λ_{BG}. For a blackbody source at 1700K, the maximum theoretical efficiency of a GaSb

PV cell is only 25.6%. Clearly, a blackbody emitter is not an ideal choice for STPV systems as it radiates a significant fraction of energy above λ_{BG}, thereby highlighting the critical need for a spectrally selective emitter and photon recycling in STPV for boosting the system efficiency. The high incident power density results in thermal stress on the PV cells. Therefore, a thermal management system, usually water-cooling, is implemented in STPV to keep the solar cells at room temperature (300 K). STPV systems are scalable, reliable (no moving parts), and versatile in utilizing alternative sources of heat, such as radioisotope heaters, thermal storage systems, combustible materials, etc., as inputs.

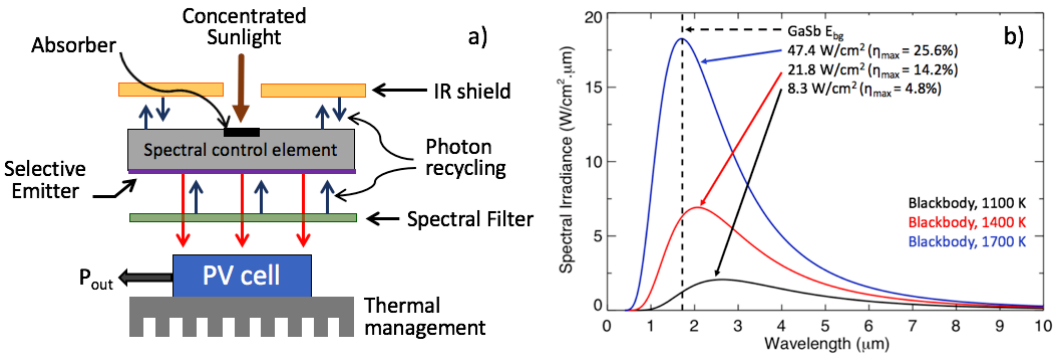

Fig. 1 (a) Layout of a typical planar STPV system. (b) impact of the spectral distribution of the blackbody power on the conversion efficiency of a GaSb PV cell.

Here, we fabricated a complete planar STPV setup using a spectrally selective emitter/absorber and GaSb PV cells. The spectral properties of emitter were optimized to maximize the output power density from the PV cells. The system was tested at different operating temperatures using simulated concentrated solar conditions and experimental results are presented.

2 State-of-the-art Review

The ultimate theoretical conversion efficiency of an ideal STPV system with no optical losses and under full solar concentration have been determined to be ~85% [9]. The derivation of the

maximum efficiency limit is based on several restrictive constraints that cannot be achieved in real STPV systems. For instance, the maximum system efficiency is achieved at an impractical solar concentration of 46000X, with a narrow monochromatic emission (matching the bandgap of the cell) from the emitter and using solar cells with no optical losses and non-radiative recombination. The narrowband monochromatic emission requires extremely large (approaching infinity) emitter area to re-radiate the absorbed solar radiation, resulting in an impractical STPV system with nearly zero output power density [10]. A realistic STPV system is required to be more compact and produce adequately high output electrical power density from practically achievable input solar concentration. Therefore, the idea of monochromatic emitter needs to be abandoned and the thermal emission from the emitter is required to have a sufficient bandwidth to maximize the open circuit voltage and impedance matching in PV cells [7]. In fact, for a given bandgap of solar cell there is an optimal non-zero emission bandwidth for which the PV conversion efficiency is maximum [7].

Previous thermodynamic simulation studies reported overall conversion efficiencies around 45% for less idealized STPV systems [7][11-12]. But, to date no experimental demonstration of a STPV system has been put forth with efficiency beyond that of a standard single-junction solar cell. Most of the early designs were based on cylindrical configurations utilizing a centered radiator surrounded by a large cavity made of solar cells [13-15]. Owing to lack of spectral selectivity in the absorber/emitter structure and low area-ratio of radiator to solar cells, their reported efficiency was poor (<1%). In 2014, A. Lenert et al. built an efficient STPV system using a vertically aligned multi-walled carbon nanotube absorber and a 1-D Si/SiO2 photonic crystal emitter [1]. This system was planar and used a narrow-bandgap InGaAsSb solar cell (0.55 eV), which allowed efficient

operation at lower system temperature (1285 K). The system was tested under simulated solar conditions and the efficiency of 3.2% was reported.

C. Ungaro et al. demonstrated a high efficiency STPV system utilizing nanostructures-based selective absorber/emitter fabricated on a W substrate and GaSb cells [2]. The reported efficiency was 6.2% at ~1700 K. Another high-efficiency planar STPV configuration using GaSb cells was presented by A. Kohiyama et al. with a measured system efficiency of 5.1% [3]. They utilized multilayer coatings of Molybdenum (Mo) and Hafnium oxide (HfO2) on a Mo substrate for constructing a selective absorber/emitter structure. The highest STPV system efficiency reported so far was achieved by pairing a tandem plasma-interference optical filter with a 1-D Si/SiO2 photonic crystal based selective emitter [4]. The filter was engineered to reflect 80% of the sub-bandgap photons back to the emitter while allowing the in-band photons to pass through. Using an InGaAsSb cell, the reported system efficiency was 6.8%.

3 Experimental Setup

A complete STPV system was designed comprising a planar absorber/emitter structure and GaSb PV cells. Tungsten (W) was chosen for the absorber/emitter substrate because it preserves its structural integrity at high temperatures and possesses good intrinsic optical properties suitable for STPV applications [14]. The absorber and emitter were fabricated on the top and bottom surfaces of a polished W substrate (Fig. 2a) purchased from MTI Corporation. The substrate was 25.4 x 25.4 x 0.5 mm in dimensions. A 0.64 cm^2 area on its top surface was micro-textured to enhance the solar absorption. For texturing, an IPG Photonics YLP-1/30 nanosecond 1064 nm pulsed laser operating with an average power of 24 W and 30 KHz frequency was scanned over the absorber surface by means of Galvo. The bottom surface of the W substrate served as emitter and was composed of a multilayer nanostructure to achieve spectral selectivity. The multilayer structure

consists of two layers of 160 nm Si_3N_4 dielectric and a 40 nm W layer sandwiched in between as shown in Fig. 2b. The film thicknesses were computed from transfer matrix method (TMM) simulation conducted to maximize the thermal emission near the λ_{BG} (1.72 μm) of GaSb. Prior to the deposition of films, the W surface was cleaned via microwave oxygen plasma cleaning. The deposition rate of the films was calibrated based on ellipsometry measurements. Silicon nitride layers were deposited by plasma-enhanced chemical vapor deposition (PECVD) method in an Oxford Plasmalab System 100 reactor using silane and ammonia gas mixture diluted in argon. The process of mixing high and low frequency powers was employed to minimize silicon nitride film stress and, at the same time, to obtain a higher film density. The substrate temperature during deposition was maintained at 300 °C. The tungsten film was sputtered onto the substrate at room temperature from a high-purity (99.95%) W target at 90W DC power and 0.67Pa Ar gas pressure. The reflectance (R) of the absorber and emitter surfaces were measured using a Varian Cary 5E Spectrophotometer that has a spectral range of 300-3300 nm. The absorptance (1-R) of the absorbing surface was found to be uniform (~92%) across the wavelength of 300-1000 nm. Figure 2c shows the simulated and measured absorptivity or emittance of the fabricated emitter. Compared to plain W, the multilayer emitter surface exhibits a better spectral selectivity with increased thermal emittance right above the bandgap of GaSb solar cell. The observed difference between the measured and simulated absorption spectra is attributed to inadequate control of the deposited film thickness as well as the deviation of the optical constants of the materials from the values used in the simulation. Ellipsometry measurements of the emitter surface revealed that the three films were over deposited by ~10-12% of the aimed thickness.

The GaSb PV cells used in this experiment were purchased from JX Crystals. The cells have an active area of $1cm^2$ each. The fill factor (FF) of the cells was measured using a quartz tungsten

halogen (QTH) lamp source and found to be 0.66. Based on the specification provided by JX Crystals, the external quantum efficiency (EQE) of the cell peaks to ~0.65 near 1.5 μm. Four such cells are mounted on a copper substrate via reflow soldering. The cell mount was actively cooled using circulating water at 10°C. The maximum conversion efficiency of the cells was determined experimentally for a matched input spectrum derived from the QTH lamp source using a 200 nm bandwidth optical bandpass filter (center wavelength at 1337 nm) purchased from PIXELTEQ. The filtered output from the lamp was calibrated using Thorlabs's PM100D power meter. The measured conversion efficiency was 26.3%, which is slightly lower than the manufacturer-reported value of ~30% for spectrally matched incident radiation.

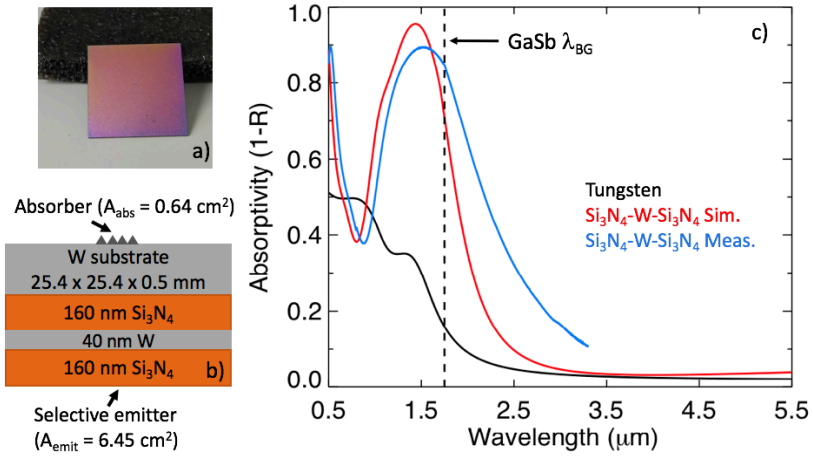

Fig. 2 (a) Picture showing the emitter side of the W substrate. (b) Schematic of the planar absorber/emitter structure. (c) Absorptivity of W and Si_3N_4-W-Si_3N_4 selective emitter (simulated in Red and measured in Blue).

Two thin fused silica rods were used to support the W substrate over the PV cells with a spacing of ~1.5 mm. The temperature of the substrate was measured using a type R thermocouple that was bonded to the substrate on the absorber side using the OB-600 high temperature chemical set cement purchased from OMEGA. A reflective heat shield was constructed using a gold foil mounted on an aluminum frame using the OB-600 cement. The shield was installed on the absorber side covering only the non-textured area of the W substrate. The spacing between the shield and

the substrate was ~2 mm. The whole STPV assembly was installed inside a vacuum chamber to minimize convective losses. A 9.5 CFM capacity 2-stage vacuum pump was run to achieve vacuum conditions of 80 mTorr. A 300 W continuous wave laser (λ=808 nm) was setup to simulate the concentrated solar radiation in the lab. The laser was focused on the 0.64 cm^2 micro-textured absorbing surface. During the experiment, the open-circuit voltage (V_{oc}) and short-circuit current (I_{sc}) of the GaSb cells were measured using multimeters. The maximum substrate temperature was recorded to be 1676 K for the incident laser power of 131 W.

4 STPV system modeling

A complete thermodynamic model was formulated to analyze the flow of power at multiple transport steps of the STPV system. For a given incident concentrated power (P_{in}), the emitter temperature at thermal equilibrium can be computed by solving the following equation.

$$P_{in} - P_{ref} - P_{rad,abs}(T) - P_{rad,side}(T) - P_{conv}(T) - P_{cond}(T) - P_{rad,emit}(T) = 0 \qquad (1)$$

where P_{ref} is the amount of power reflected off the absorbing surface, $P_{rad,abs}(T)$ is the thermally radiated power from the absorbing surface, $P_{rad,\,side}(T)$ is the power loss due to radiation from the 4 sides of the W substrate, $P_{conv}(T)$ is the convective power loss, $P_{cond}(T)$ is the conduction loss due to silica rods and thermocouple, and $P_{rad,emit}(T)$ is the net radiant flux emitted from the emitter surface. Because the incident power in this setup is monochromatic, P_{abs} is approximately 92% of P_{in} (P_{ref}=~8% of P_{in} at the laser wavelength based on the reflectance measurements of the microtextured W area). The radiant flux emitted from the absorber surface ($P_{rad,abs}$) consists of two components: one radiated from a highly emissive microtextured area (A_{abs}=0.64 cm^2), and second from the inactive or non-textured W area (5.81 cm^2). The thermal radiation emitted from a surface can be computed from Planck's function and the spectral emissivity of the surface. In our simulation, the emissivity of the involved surfaces is simply assumed to be (1-Reflectivity). The

reflectance spectra of W were derived using the optical constants provided by Rakic et al [16], whereas the reflectance of the microtextured area was measured. $P_{rad,\ side}$ is computed in the similar way using the emissivity of W. $P_{conv}(T)$ is simulated using equations for natural convection above a horizontal surface provided in literature [17]. The conduction loss (P_{cond}) from support was computed using fin approximation equations as described by A. Lenert et al. [1]. Finally, the radiant flux power $P_{rad,emit}$ from the emitter surface was estimated using Planck's blackbody equation and the measured spectral emissivity of the surface.

One commonly used figure of merit to assess the performance of an STPV absorber/emitter is the thermal extraction efficiency (η_e), which is given by Eq. (2) To achieve high STPV system efficiency, η_e, which defines the fraction of the incident power that is delivered by the emitter to PV cells, must be maximized. η_e is governed by both spectral and geometric properties of the absorber and emitter [18]. Reducing the reflection and emission losses from the absorber surface, and meanwhile, maximizing the emissivity of the emitter surface can yield in a high η_e value. The absorber-side emission losses can be suppressed by keeping the absorber area small compared to that of emitter [18]. The geometric control of η_e is, therefore, defined by emitter-to-absorber area ratio (AR), which is 10 in our experimental setup.

$$\eta_e = \frac{P_{rad,emit}}{P_{in}} \tag{2}$$

High η_e is necessary but not sufficient to ensure a high STPV system efficiency. Because PV cells only responds to a limited wavelength range, it is important that the thermal emission from the emitter matches the spectral response of the cells. This characteristic of emitter is known as spectral selectivity (η_{sel}) and is defined as follows.

$$\eta_{sel} = \frac{\int_0^{\lambda_{BG}} \varepsilon(\lambda) B(\lambda,T) d\lambda}{\int_0^{\infty} \varepsilon(\lambda) B(\lambda,T) d\lambda} \quad (3)$$

where $\varepsilon(\lambda)$ is the emissivity of the selective emitter, $B(\lambda, T)$ is Planck's blackbody function, and λ_{BG} is the bandgap wavelength of GaSb.

In addition to high spectral selectivity, the emitter also needs to have a large effective in-band emissivity ($\varepsilon_{in\text{-}band}$), defined by Eq. 4, for maximal radiant flux power density that directly affects the PV cell output. Table 1 summarizes η_{sel}, $\varepsilon_{in\text{-}band}$, and $P_{rad,emit}$ for W, blackbody, and Si_3N_4-W-Si_3N_4 emitters. Tungsten exhibits an excellent η_{sel} but poor $\varepsilon_{in\text{-}band}$. A blackbody emitter provides maximum in-band emission but its spectral selectivity is only 24.7%. Based on the simulated reflectance spectra, the Si_3N_4-W-Si_3N_4 emitter offers high values of η_{sel} (66.1%) and $\varepsilon_{in\text{-}band}$ (0.84). η_{sel} is reduced to ~53% in the fabricated emitter sample due to the limited tolerances in the film thicknesses. The in-band radiant flux emitted by Si_3N_4-W-Si_3N_4 is nearly 3 times greater than that of W.

$$\varepsilon_{in-band} = \frac{\int_0^{\lambda_{BG}} \varepsilon(\lambda) B(\lambda,T) d\lambda}{\int_0^{\lambda_{BG}} B(\lambda,T) d\lambda} \quad (4)$$

Table 1 Spectral selectivity, in-band emissivity, and radiant flux density computed for different emitting surfaces at T=1676 K.

Emitter Type	η_{sel} (%)	$\varepsilon_{in\text{-}band}$	$P_{rad,emit}$ (W/cm^2)
Tungsten	69.2	0.33	5.19
Blackbody	24.7	1.00	44.73
Si_3N_4-W-Si_3N_4 Simulated	66.1	0.84	13.98
Si_3N_4-W-Si_3N_4 Measured	52.6	0.81	18.89

An additional efficiency gain can be achieved by photon recycling that occurs in our STPV design on both absorber and emitter sides. The high reflectivity of the gold shield recycles the

thermal radiation from the inactive absorber area back to the W substrate. The effective emittance of the inactive W area in the presence of the reflector can be modeled by Eq. 5 [3,19], and subsequently used to simulate the suppressed emission losses. In our experimental setup, no dedicated spectral filter was installed in between the PV cells and the emitter for recycling of the sub-bandgap emission. However, some sub-bandgap photons are reflected back to the emitter due to the non-zero reflectance of the cells at longer wavelengths. The reflectance of the cell is characterized using the spectrophotometer, and is found to be ~5% (after accounting for the reflectance from the silver grid bars on the cells) near 1.4 μm, and up to 45% at sub-band wavelengths. The recycling effect on the emitter side was modeled in a similar way as for the absorber side using Eq. 5. Simulation results show that the installation of the heat shield suppressed the thermal loss from the absorber side by 61%, while the cell reflectance resulted in the average sub-bandgap reflectivity of 35%.

$$\varepsilon_{Eff} = \left(\frac{1}{\varepsilon_W} + \frac{1}{1-\varepsilon_{Au}} \right)^{-1} \tag{5}$$

The overall STPV system efficiency (η_{STPV}) is modeled as:

$$\eta_{STPV} = \eta_e . \eta_{sel} . \eta_{PV} \tag{6}$$

where η_{PV} is the conversion efficiency of the GaSb cell. The short-circuit current density (J_{sc}) is modeled by integrating the absorbed photon flux across wavelengths less than λ_{BG}. The external quantum efficiency (EQE) data required for computing J_{sc} was provided by JX Crystals. The reverse saturation current density and V_{oc} of the GaSb cell as well as their dependence on cell temperature was modeled using equations and constants provided by L. Ferguson et al. [20]. Not all the radiation leaving the emitter surface reaches the cells due to a finite spacing between the two. A radiative view factor (VF) between the emitter and TPV cell areas is computed to be 0.91,

which implies that 9% of the energy radiated by emitter is not intercepted by the cells. This is referred as cavity loss. The measured absorption spectra of the absorber and emitter surfaces were used for quantitative analysis of thermal radiation in the simulation.

When a concentrated solar radiation is incident on the absorber surface, the temperature of the absorber/emitter structure increases until thermal equilibrium is reached. The simulated steady-state absorber/emitter temperature for a given input laser power is shown in Fig. 3a. The black curve shows a case of no photon recycling. For the same input power, the STPV equilibrium temperature goes up with the installation of the gold reflector over the inactive region of the W absorber, as shown by the red curve. The combined effect of photon recycling due to the heat shield and the reflection off the GaSb cells is illustrated by the green curve. The simulation results show that the input solar concentration required to achieve the steady-state temperature of 1676 K reduces from 2718 to 1996 due to the combined photon recycling. The thermal extraction efficiency as a function of AR is plotted in Fig. 3b. The presence of the gold reflector leads to an improved η_e. For AR=10 (current experimental setup), the modeled η_e is ~78%. Fig. 3d shows the comparison between the simulated J_{sc} computed for a GaSb cell using a blackbody emitter (Green) and Si_3N_4-W-Si_3N_4 selective emitter (Red) as a function of the emitter temperature. J_{sc} for the selective emitter is lowered by a factor of $\varepsilon_{in\text{-}band}$ =0.81. The simulated losses at different stages of energy transport in our STPV system operating are summarized in Table 2 for T=1676 K.

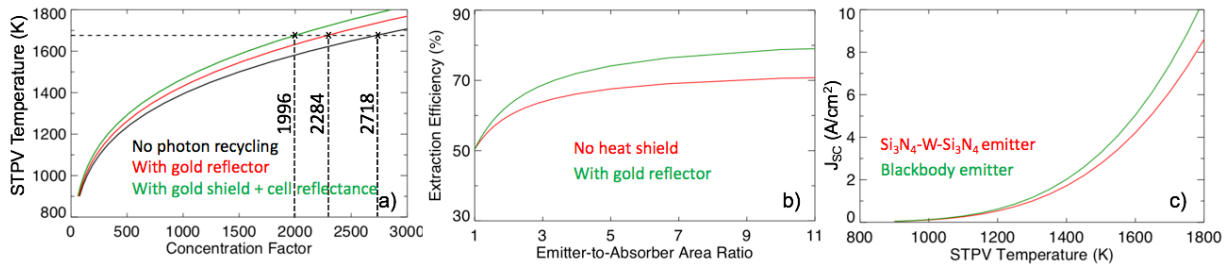

Fig. 3 (a) Simulated steady-state absorber/emitter temperature as a function of incident solar concentration. Black curve represents a case of no photon recycling. Effect of the gold reflector over the inactive area of the absorber is shown in Red. Green curve shows the combined effect of photon recycling on both absorber and emitter sides. (b)

Simulated extraction efficiency as a function of AR with (Green) and without (Red) the gold reflector. (c) Simulated J_{sc} as a function of STPV temperature for a blackbody (Green) and our selective emitter (Red).

Table 2 Modeled power losses at each stage of the experimental STPV system operating at T=1676 K.

Loss item	Percent of input power
Reflection off the absorber	8%
Emission from absorber side	11.9%
Emission from sides	2.1%
Convective loss	2.5%
Conduction loss	1.0%
Cavity loss due to VF	8.3%
Sub-bandgap loss	29.6%
TPV conversion loss	19.0%
Thermalization loss	8%
Output electrical power	9.6%

4 Experimental results

The STPV system was tested at various levels of incident laser power, and the corresponding absorber/emitter temperature and PV cell output were recorded. Modeled and measured PV cell output power and system efficiency at different STPV temperatures are shown in Fig. 4. With increasing temperature, the thermal emission from the emitter not only increases but also exhibits better spectral matching with the EQE of the PV cell, thereby resulting in an exponential increment in the PV cell output and improved system efficiency. Both the measured PV cell output and system efficiency follows the simulation curves closely. The maximum cell output power density of 1.71 W/cm^2 and overall system efficiency of 8.4% were recorded at a temperature of 1676K. The corresponding incident laser power was 131 W. This value is close to the simulated P_{in} value of 126 W, thereby confirming the robustness of the simulation models. The 131 W laser beam was focused on the 0.64 cm^2 absorber area is equivalent to a solar concentration factor of 2060 (assuming air mass of 1.5), which is within the practical limit and is achievable with Fresnel lens setup. The modeled system efficiency at 1676K temperature is 9.6%. The slight difference between

the modeled and measured system efficiency is attributable to simplified approximations incorporated at various stages of simulation.

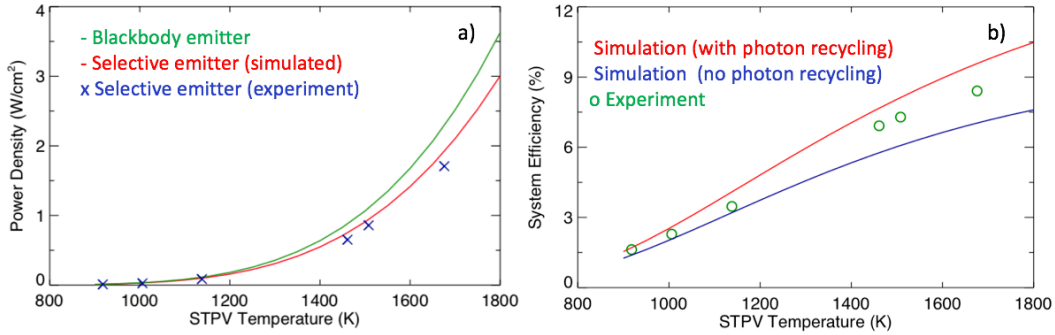

Fig. 4 (a) Experimental (Blue points) and simulated (Green curve for blackbody emitter and Red curve for our selective emitter) TPV cell output power at various absorber/emitter temperatures. (b) Modeled (Blue curve is for no photon recycling and Red curve is with photon recycling) and experimental (Green points) STPV system efficiency obtained at various operating temperatures.

The PV cell temperature rose to 316K that resulted in a 5% drop in V_{oc}. For the matched portion ($\lambda<\lambda_{BG}$) of the spectral emission from the emitter, η_{PV} =18% was achieved at 1676K. This is lower than η_{PV} =26% measured with a narrowband emission from the QTH lamp and filter setup. This significant reduction in experimental η_{PV} is due to increased thermalization loss at shorter wavelengths. The high sub-bandgap emission causes the greatest system efficiency loss (~30%) in our design. η_{sel} must be improved for suppressing the sub-bandgap loss. If the simulated spectral emission of the Si_3N_4-W-Si_3N_4 structure had been achieved for the fabricated sample, the sub-bandgap loss would have reduced by ~50% and the system efficiency would rise to 11%. Additionally, a selective window filter can also be installed in between the emitter and PV cell for more effective recycling of sub-bandgap photons. This filter needs to be transmitive to in-band radiation, and highly reflective at wavelengths >λ_{BG}. Previous studies have reported resonance and plasma-interference filter structures based on semiconductors and transparent conducting oxides as potential edge filters for photon recycling in STPV systems [21-23]. Alternatively, re-utilization of sub-bandgap photons can also be achieved using metal reflectors at the back interface of PV cells. Recently, Z. Omair et al. reported 94% sub-bandgap reflectivity achieved by utilizing the

photovoltaic band-edge as spectral filter and incorporating a rear gold reflector in a lattice-matched $In_{0.53}Ga_{0.47}As$ PV cell [24]. A 75% reduction in the sub-bandgap loss in the current system would provide an additional gain of 2.4% in the system efficiency.

Second major loss factor is PV conversion loss (19%) in GaSb cells, which resulted mostly due to poor practical values of FF and EQE compared to much higher theoretical values reported by the manufacturer team in [18]. The difference between the theoretical and practical values of FF and EQE resulted in a 3% reduction of η_{STPV}. The reflection loss from the absorber surface was found to be 8%. Reducing it to 1% would further add 0.6% gain in the system efficiency. Therefore, future works should be focused on suppressing the sub-bandgap radiation, using better TPV cells, and reducing the reflection loss. The combination of these improvements would lead to an enhanced system efficiency of 14.5% for our planar STPV system.

4 Conclusion

In summary, we designed and tested a high-efficiency planar STPV system using a micro-textured absorber and a multilayer metal-dielectric (Si_3N_4-W-Si_3N_4) coating-based selective emitter. High thermal extraction and effective recycling of the sub-bandgap photons are key to achieve high system efficiency. We implemented a gold-based heat shield that suppressed the undesired thermal emission from the absorber side by ~61%. A system efficiency of 8.4% was achieved from the fabricated absorber/emitter at the system temperature of 1676K and incident solar concentration of 2060. Our experimental efficiency is higher than those of previously reported STPV systems and this can be improved further by incorporating a better recycling scheme to reflect unconvertable photons back to the emitter and by using more efficient GaSb cells.

Acknowledgments

We thank the NASA Langley Professor program and NSF IUCRC Center for the financial support. A portion of this research was conducted at the Center for Nanophase Materials Sciences, which is sponsored at Oak Ridge National Laboratory by the Scientific User Facilities Division, Office of Basic Energy Sciences, U.S. Department of Energy.

References

1. A. Lenert, D. M. Bierman, Y. Nam, W. R. Chan, I. Celanovic, M. Soljacic, and E. N. Wang, "A nanophotonic solar thermophotovoltaic device," *Nature Nanotech.* 9, 126–130 (2014).
2. C. Ungaro, S. K. Gray, and M. C. Gupta, "Solar thermophotovoltaic system using nanostructures," *Opt. Express* 23, A1149 (2015).
3. A. Kohiyama, M. Shimizu, and H. Yugami, "Unidirectional Radiative Heat Transfer with a Spectrally Selective Planar Absorber/Emitter for High-efficiency Solar Thermophotovoltaic Systems," *Appl. Phys. Exp.* 9(11), 112302 (2016).
4. D. M. Bierman, A. Lenert, W. R. Chan, B. Bhatia, I. Celanović, M. Soljačić, and E. N. Wang, "Enhanced photovoltaic energy conversion using thermally based spectral shaping," *Nat. Energy* 1(6), 16068 (2016).
5. W. Shockley and H. J. Queisser, "Detailed balance limit of efficiency of p-n junction solar cells," *J. Appl. Phys.* 32, 510–519 (1961).
6. S. Rühle, "Tabulated values of the Shockley–Queisser limit for single junction solar cells," *Solar Energy.* 130: 139–147 (2016).
7. E. Rephaeli and S. Fan, "Absorber and emitter for solar thermo-photovoltaic systems to achieve efficiency exceeding the Shockley-Queisser limit," *Opt. Express* 17, 15145-15159 (2009).
8. A. Datas, "Optimum semiconductor bandgaps in single junction and multijunction thermophotovoltaic converters," *Solar Energy Materials and Solar Cells* 134, 275-290 (2015).

9. N. P. Harder and P. Wurfel, “Theoretical limits of thermophotovoltaic solar energy conversion,” *Semicond. Sci. Technol*. 18(5), S151–S157 (2003).
10. A. Datas and C. Algora, "Global optimization of solar thermophotovoltaic systems", *Prog. Photovoltaics Res. Appl.*, vol. 21, no. 5, pp. 1040-1055 (2013).
11. Y. Nam, A. Lenert, Y. X. Yeng, P. Bermel, M. Soljacic, and E. N. Wang, “Solar thermophotovoltaic energy conversion systems with tantalum photonic crystal absorbers and emitters,” *Transducers and Eurosensors CCVII: The 17th International Conference*, pp. 1372-1375 (2013).
12. P. Bermel, M. Ghebrebrhan, W. Chan, Y. X. Yeng, M. Araghchini, R. Hamam, C. H. Marton, K. F. Jensen, M. Soljacic, J. D. Joannopoulos, S. G. Johnson, and I. Celanovic, “Design and global optimization of high-e_ciency thermophotovoltaic systems,” *Optics Express*, 18, A314-A334 (2010).
13. H. Yugami, H. Sai, K. Nakamura, H. Nakagawa, and H. Ohtsubo, “Solar thermophotovoltaic using $Al_2O_3/Er_3Al_5O_{12}$ eutectic composite selective emitter,” *IEEE Photovoltaic Specialists Conference* 28, 1214– 1217 (2000).
14. A. Datas and C. Algora, “Development and experimental evaluation of a complete solar thermophotovoltaic system,” *Progress in Photovoltaics: Research and Applications* 890, 327–334 (2012).
15. A. S. Vlasov, V. P. Khvostikov, O. A. Khvostikova, P. Y. Gazaryan, S. V. Sorokina, and V. M. Andreev, “TPV systems with solar powered tungsten emitters,” *AIP Conference Proceedings* 890, 327–334 (2007).
16. A. D. Rakić, A. B. Djurišic, J. M. Elazar, and M. L. Majewski, “Optical properties of metallic films for vertical-cavity optoelectronic devices,” *Appl. Opt.* **37**, 5271-5283 (1998).
17. Z. Rotem and L. Classen, “Natural convection above unconned horizontal surfaces,” *Journal of Fluid Mechanics* 38, 173-192 (1969).
18. A. Kohiyama, M. Shimizu, and H. Yugami, “Radiative heat transfer enhancement using geometric and spectral control for achieving high-efficiency solar-thermophotovoltaic systems,” *The Japan Society of Applied Physics* (2018).

19. A. Lenert, Y. Nam, D. M. Bierman, and E. N. Wang, "Role of spectral non-idealities in the design of solar thermophotovoltaics," *Opt. Express* 22, A1604-A1618 (2014)
20. L. Ferguson and L. Fraas, “Theoretical study of GaSb PV cells efficiency as a function of temperature,” *Solar Energy Mater. Solar Cell*, 39 pp. 11-18, (1995)
21. M. Zenker, A. Heinzel, G. Stollwerck, J. Ferber, and J. Luther, “Eflciency and power density potential of combustion-driven thermophotovoltaic systems using GaSb photovoltaic cells,” *IEEE Trans Electron Devices*, 48, 367–376 (2001).
22. O. Vigil, C. M. Ruiz, D. Seuret, V. Bermúdez, and E. Diéguez E, “Transparent conducting oxides as selective filters in thermophotovoltaic devices,” *J Phys Condens Matter*, 17, 6377–6384 (2005).
23. Z. G. Qian, W. Z. Shen, H. Ogawa, and Q. X. Guo, “Infrared reflection characteristics in InN thin films grown by magnetron sputtering for the application of plasma filters,” *J Appl Phys* 92, 3683 (2012).
24. Z. Omair et al., "Experimental Demonstration of 28.2% Thermophotovoltaic Conversion Efficiency," *2018 Conference on Lasers and Electro-Optics (CLEO)*, San Jose, CA, pp. 1-2 (2018).

Caption List

Fig. 1 (a) Layout of a typical planar STPV system. (b) impact of the spectral distribution of the blackbody power on the conversion efficiency of a GaSb TPV cell.

Fig. 2 (a) Picture showing the emitter side of the W substrate. (b) Schematic of the planar absorber/emitter structure. (c) Absorptivity of W and Si_3N_4-W-Si_3N_4 selective emitter (simulated in Red and measured in Blue).

Fig. 3 (a) Simulated steady-state absorber/emitter temperature as a function of incident solar concentration. Black curve represents a case of no photon recycling. Effect of the gold reflector over the inactive area of the absorber is shown in Red. Green curve shows the combined effect of photon recycling on both absorber and emitter sides. (b) Simulated extraction efficiency as a

function of AR with (Green) and without (Red) the gold reflector. (c) (d) Simulated J_{sc} as a function of STPV temperature for a blackbody (Green) and our selective emitter (Red).

Fig. 4 (a) Experimental (Blue points) and simulated (Green curve for blackbody emitter and Red curve for our selective emitter) TPV cell output power at various absorber/emitter temperatures. (b) Modeled (Blue curve is for no photon recycling and Red curve is with photon recycling) and experimental (Green points) STPV system efficiency obtained at various operating temperatures.

Table 1 Spectral selectivity, in-band emissivity, and radiant flux density computed for different emitting surfaces at T=1676 K.

Table 2. Modeled power losses at each stage of the experimental STPV system operating at T=1676 K.